Journal of Colloid and Interface Science 702 (2026) 138806

Contents lists available at ScienceDirect

Journal of Colloid And Interface Science

journal homepage: www.elsevier.com/locate/jcis

Ferromagnetic ferrofluids in aqueous and low-polar media

Jošt Truč[a,b,*,1], Patricija Hribar Boštjančič[c,1], Žiga Gregorin[c], Peter Medle Rupnik[c], Alenka Mertelj[c], Darja Lisjak[a]

[a] Department for Materials Synthesis, Jožef Stefan Institute, Jamova cesta 39, 1000 Ljubljana, Slovenia
[b] Jožef Stefan International Postgraduate School, Jamova cesta 39, 1000 Ljubljana, Slovenia
[c] Department of Complex Matter, Jožef Stefan Institute, Jamova cesta 39, 1000 Ljubljana, Slovenia

HIGHLIGHTS

- Aqueous and low-polar ferromagnetic ferrofluids were developed.
- Liquid magnets form at sufficiently high concentrations of magnetic nanoplatelets.
- Magnetic nanoplatelets spontaneously assemble into a ferromagnetic nematic phase.
- Colloidal repulsive interactions equilibrate the magnetic dipolar attraction.

GRAPHICAL ABSTRACT

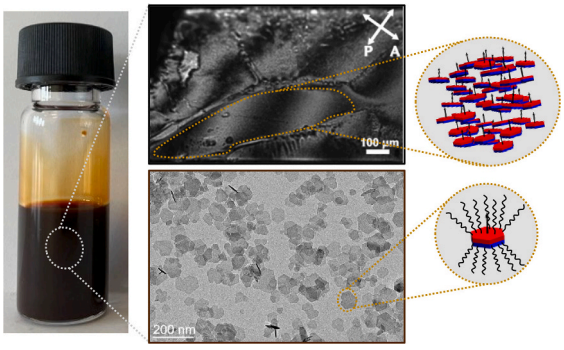

ARTICLE INFO

Keywords:
Liquid magnet
Ferrofluid
Barium hexaferrite nanoplatelets
Low-polar
Aqueous media

ABSTRACT

Currently known ferromagnetic ferrofluids (FFs), or liquid magnets, are typically composed of permanently magnetic barium hexaferrite nanoplatelets (BHF NPLs) dispersed in 1-butanol, where colloidal stability is achieved through electrostatic repulsion. Here, we report the development of an environmentally friendly, water-based ferromagnetic ferrofluid, in which magnetic dipolar attractions are effectively suppressed by a synergistic combination of electrostatic, steric, and hydration repulsion. We further demonstrate that stable ferromagnetic ferrofluids can also be realized in low-polarity organic solvents such as dichloromethane (DCM) and 1-hexanol, relying solely on sufficient steric–solvation repulsion—without the need for long-range electrostatic repulsion. These different types of ferromagnetic FFs offer a promising platform for tubeless microfluidic pumping in diverse chemical systems.

1. Introduction

Ferromagnetic ordering in liquids is a rare phenomenon. Apart from exotic systems observed at cryogenic [1] and elevated temperatures [2], only two types of colloidal nematic ferromagnetic liquids have been realized under ambient conditions [3,4], even though Brochard and de

* Corresponding author at: Department for Materials Synthesis, Jožef Stefan Institute, Jamova cesta 39, 1000 Ljubljana, Slovenia.
E-mail address: jost.trucl@ijs.si (J. Truč).
[1] Author 1 and Author 2 contributed equally to this work.

https://doi.org/10.1016/j.jcis.2025.138806
Received 23 July 2025; Received in revised form 12 August 2025; Accepted 22 August 2025
Available online 25 August 2025

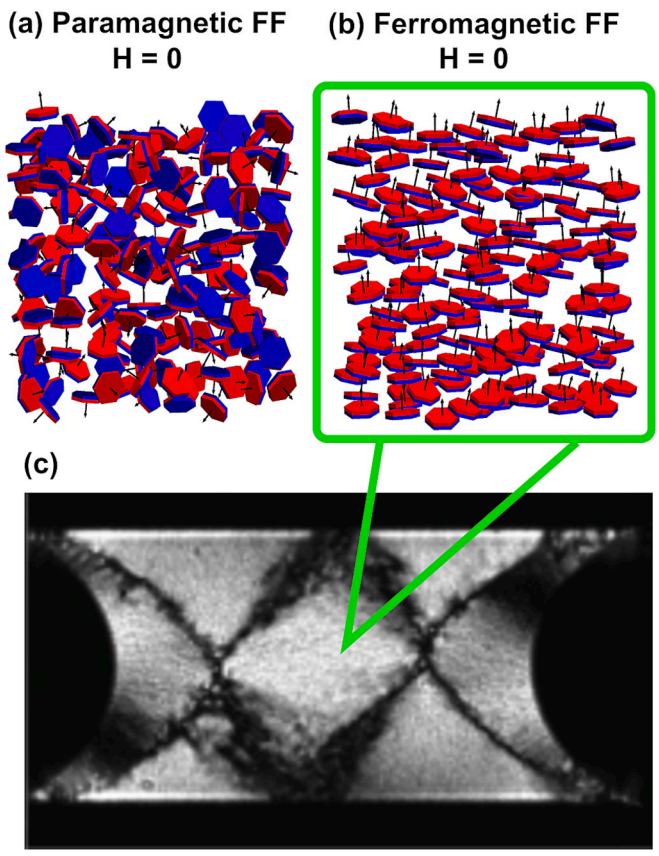

Scheme 1. Schematic presentation of dispersed magnetic NPLs in the absence of an external magnetic field (H = 0): (a) (super)paramagnetic FF with no orientational ordering and (b) ferromagnetic FF, where the NPLs orientationally order with their magnetic dipoles aligned in the same direction, i.e., the sample exhibits spontaneous magnetization. (c) Polarizing optical microscopy (POM) photograph of a 1-butanol suspension of magnetic NPLs placed in a layer confinement (capillary thickness is 30 μm), showing a typical domain formation in the absence of an external field.

Gennes [5] had predicted a ferromagnetic order in nematic liquid crystals many years beforehand. Numerous studies [6–8] utilizing spherical or rod-like magnetic particles failed to realize the predicted ferromagnetic liquid. The isotropic magnetic properties of spherical particles and the preferred antiferromagnetic assembly of rod-like particles do not allow for a ferromagnetic coupling [9].The key ingredients of nematic ferromagnetic liquids are magnetic nanoplatelets (NPLs) with a rare combination of uniaxial magnetocrystalline and shape anisotropy directing the magnetic easy axis perpendicular to their basal plane. Consequently, by equilibrating the colloidal and magnetic dipolar interactions, such magnetic NPLs can ferromagnetically couple in a liquid system.

The magnetic NPLs in the two known colloidal ferromagnetic systems are Sc-substituted barium hexaferrite (BSHF) NPLs functionalized with a surfactant dodecylbenzenesulfonic acid (DBSa). In the ferromagnetic liquid-crystalline suspension, the NPLs were dispersed in a liquid-crystalline matrix, where ferromagnetic coupling is induced through alignment mediated by molecular orientational order [3]. Similar to this, a ferroelectric liquid crystal with ferromagnetic order was only recently developed from the BSHF NPLs functionalized with DBSa [10]. In contrast, in the isotropic solvent, the combination of NPLs' shape and magnetic interaction induces ferromagnetic nematic ordering in a highly concentrated suspension of the NPLs in 1-butanol, yielding a ferromagnetic ferrofluid (FF) [4]. The defining characteristic of such ferromagnetic FFs is the formation of magnetic domains in the absence of an external magnetic field (H = 0) (Scheme 1). These ferromagnetic FFs exhibit extreme sensitivity to magnetic fields, responding even to fields comparable to the Earth's magnetic field [11].

Optimization of the system BSHF NPLs–DBSa–alcohols [12,13] demonstrated that the ferromagnetic nematic phase can form at substantially lower NPLs concentrations (≈ 5 vol%) than initially reported (28 vol%) [4]. In such FFs, a delicate balance between the repulsive electrostatic and attractive ferromagnetic forces is responsible for the suspensions' colloidal stability and the ferromagnetic ordering. Recent work has further revealed that an oscillatory magnetic field causes chiral symmetry breaking and drives a macroscopic flow [14]. The flow lanes appear due to the spontaneous ordering and collective rotation of the magnetic NPLs within magnetic domains. The coupling between magnetic ordering and fluid motion opens opportunities for tubeless microfluidic actuation—a mechanism that contrasts with previously proposed approaches based on traveling-wave-driven ferrohydrodynamic pumping in paramagnetic FFs composed of spherical particles [15,16]. However, the use of 1-butanol, being a highly volatile solvent, limits the implementation of these FFs in microfluidics. A reasonable alternative to 1-butanol would be water.

When the NPLs are functionalized with DBSa in water, they flocculate because DBSa does not form a double layer as it does in certain alcohols [17]. The BSHF NPLs can be dispersed in aqueous media either in nitric acid solutions at pH < 4 or at neutral-to-basic pH when functionalized with citric acid or coated with an amorphous silica shell [18]. However, the resulting concentrations are too low to support ferromagnetic ordering. As an alternative, phosphonic acid ligands are considered due to their strong affinity for metal oxide surfaces [19,20]. For electrostatic stabilization in water, a phosphonic acid bearing an additional polar group—such as a second phosphonic or sulfonic moiety—can be employed. The phosphonic group anchors to the NPL surface, while the free polar group imparts surface charge. Yet, these double-polar ligands tend to associate via hydrogen bonding and electrostatic interactions in water, which limits the ability to control their surface assembly [21]. To address this challenge, we selected a phosphonic polyether ligand. Ethers, unlike amphiphiles with alkyl chains, do not form bilayers and are well hydrated by water through hydrogen bonds [22,23]. As we show, in addition to electrostatic stabilization, a hydrated polyether tail provides sufficient steric repulsion to enable the formation of aqueous ferromagnetic FFs.

Beyond aqueous systems, we also investigated whether the ferromagnetic ordering of the BSHF NPLs can be achieved without a long-range electrostatic repulsion. We hypothesized that a combination of steric and solvation-based repulsion could stabilize BSHF NPLs in low- or non-polar solvents at concentrations high enough to support ferromagnetic ordering. This steric–solvation mechanism is validated experimentally. Specifically, we demonstrate the formation of ferromagnetic FFs by concentrating BSHF NPLs functionalized with a fatty acid in low-polar solvents such as dichloromethane (ε = 8.93) and 1-hexanol (ε = 13.30).

2. Materials and methods

2.1. Chemicals

Iron (III) nonahydrate (Alfa Aesar, >98 % for BHSF-a, and Carlo Erba reagents, >98 %, for BHSF-b), barium nitrate (Alfa Aesar, 99.95 % for BSHF-a and Chem-Lab, > 99 % for BHSF-b), scandium (III) nitrate hydrate (Alfa Aesar, 99.9 % for BSHF-a and ThermoFisher, 99.9 % for BSHF-b), sodium hydroxide (Alfa Aesar, 98 % for BHSF-a, and Carlo Erba reagents for BSHF-b), nitric(V) acid (Sigma-Aldrich, 65 %), chloroform (Sigma Aldrich, ≥ 99.8 %), dichloromethane, (J. T. Baker, > 99.5 %), methanol (Carlo Erba reagents, ≥ 99.9 %), ammonia solution (Merck for BSHF-a, 25 % and J. T. Baker, 25 % for BSHF-b), ricinoleic acid (RA) (Tokyo Chemical Industry Co. Ltd., > 80 %), and (2-{2-[2-methoxy-ethoxy]-ethoxy}-ethyl)phosphonic acid (Pether) (Sikemia, ≥ 97 %).

2.2. Magnetic NPLs

BSHF NPLs were synthesized using our established hydrothermal method [24] starting with metallic nitrates with an atomic ratio of Ba:Fe:Sc = 1:4.5:0.5 and an excess of NaOH. The reaction slurry was heated (3 °C/min) in an Inconel autoclave (Parr Instrument Co.) to 245 °C and immediately cooled down. In a typical procedure, the as-synthesized NPLs are washed three times with water and once with the nitric acid solution (pH = 0.77). The NPLs were finally dispersed in the nitric acid solution at a pH of about 2.5. These NPLs will be named BSHF-a.

Alternatively, the as-synthesized NPLs were washed 7 times with water and finally dispersed in water at pH 10–11. These NPLs will be named BSHF-b. If needed for the analysis, the NPLs were dried in air at ~80 °C.

2.3. Preparation of the aqueous ferromagnetic FF

The aqueous dispersion of BSHF-a NPLs (47 mg) was diluted to 180 ml (0.26 g/l) and 20 ml of an aqueous solution of Pether (4.3 mM ~ 10 molecules/nm^2) was added to the dispersion. The pH of the mixture was adjusted to pH 4 with the nitric-acid solution. The mixture was heated to 60 °C and stirred overnight. The BSHF-a@Pether NPLs were sedimented at 11000 RCF for 20 min, washed twice with water, and finally dispersed in water. The dispersion was concentrated in a vial using a NdFeB magnet for 2–3 weeks. After that, it was transferred to a capillary and additionally concentrated into a ferromagnetic nematic phase using a permanent NdFeB magnet.

2.4. Preparation of the nonpolar ferromagnetic FF

The BSHF-b NPLs were functionalized with ricinoleic acid (RA) following a procedure similar to that described in [25]. For the DCM dispersion, 250 mg of BSHF-b NPLs were dispersed in 50 ml of water and diluted to a concentration of 5 g/l. The pH of the dispersion was adjusted to 10–11 using a 25 % aqueous ammonia solution. The dispersion was then heated to 60 °C, and 250 mg of RA dissolved in 3 ml of methanol was added dropwise over the course of 30 min. The mixture was stirred for an additional 30 min at 60 °C, with the pH maintained at approximately 10 using the 25 % aqueous ammonia solution as necessary. For the 1-hexanol-based functionalization, the same procedure was followed with doubled quantities: 500 mg of BSHF-b NPLs dispersed in 100 ml of water, and 500 mg of RA dissolved in 6 ml of methanol. After functionalization, 1l of DI water was added to the mixture, and the pH was adjusted to 3.5 using nitric acid.

In both cases, after slowly stirring the acidic mixture for 2 h, the BSHF-b@RA particles agglomerated and were collected with a permanent magnet. Next, they were washed twice with methanol and separated using a centrifuge (Eppendorf 5804) at 3000 RCF for 5 min. Lastly, the particles were dispersed in 5 ml of dichloromethane or 1-hexanol.

2.5. Characterization of FFs

The magnetic NPLs were analysed with a transmission electron microscope (TEM, Jeol 2100) at 200 kV. The chemical composition of the NPLs was confirmed with an energy dispersive X-ray spectrophotometer (EDXS; JED 2300 EDS) coupled with the TEM. We compared the diameter-size distributions of the NPLs in the original aqueous suspension with those from the ferromagnetic FFs with the equivalent diameters determined from the TEM images using DigitalMicrograph Gatan Inc. software. We accounted for at least 250 particles for reliable statistics. The room-temperature magnetic properties were measured using dried NPLs with a vibrating-sample magnetometer (VSM, Lakeshore 7400).

The mass fraction of the functionalizing ligands and other adsorbents was determined with thermogravimetric analysis (TGA) of the dried functionalized NPLs combined with differential scanning calorimetry (DSC) and mass spectrometry (MS). Measurements were performed using TGA/DSC 2 Mettler Toledo with MS, Thermostar300 Vacuum Pfeifer (the BSHF-a samples) or NETZSCH STA 449C/6/G Jupiter–QMS 403 (the BSHF-b samples). The measurements were carried out at 40–1400 °C with a heating rate of 20 °C/min in a static air atmosphere (the BHSF-a samples) or at 35—1000 °C with a rate of 10 °C/min in an air-like mixture of argon and oxygen (the BSHF-b samples). The mass fraction of the adsorbed species on the core BSHF-a NPLs was determined from the total mass loss. In the BSHF-b NPLs, the mass fraction of nonmagnetic species was summed from the (i) mass loss at 35–400 °C, (ii) leftover of excessive NaOH determined from the mass loss of water at 400–900 °C and (iii) mass fraction of $BaCO_3$ correlated with the mass loss due to evaporation of CO_2 at the temperature interval 900–1000 °C [26]. The mass fraction of RA in the BSHF-b@RA was determined from the mass loss at 150–400 °C. The mass fraction of Pether in the BSHF-a@Pether NPLs was determined from the TGA as previously in [27], taking into account, an incomplete decomposition of the phosphonic ligand.

The presence of ligands in the functionalized NPLs was analysed with Fourier transform infrared (FTIR) spectroscopy using a PerkinElmer Spectrum 400 FT-IR/FT-FTIR spectrometer. Spectra were taken with a Universal attenuated total reflectance (ATR) accessory at 4000–650 cm^{-1} or in a diffuse reflectance infrared Fourier transform (DRIFT) mode at 4000–450 cm^{-1}.

The FFs were visually monitored for any potential sedimentation of the NPLs. In addition, the zeta-potential behaviour of the diluted aqueous FFs was determined at different pH values with Litesizer 500 (Anton Paar, Austria). The pH was adjusted with 0.01–1 M HCl or NaOH. The zeta-potential values were calculated from the measured electrophoretic mobilities using Henry's Eq. [28]. In contrast, a negligible zeta potential was expected in the low-polar suspensions. Therefore, the colloidal stability of the low-polar FFs' was assessed by measuring the solvodynamic size by dynamic light scattering (DLS) using Anton Paar, Litesizer 500. For the DLS measurement, the FFs were diluted to a maximum concentration of 1 g/l.

Orientational ordering of the suspended NPLs was examined by polarizing optical microscopy (POM). In case of randomly oriented NPLs the sample appeared dark under crossed polarisers, while in case of orientational ordering, the sample became birefringent, evidenced by observation of transmitted light. The ferromagnetic nature of the suspension was determined by three criteria. First, the suspension remained birefringent as the magnetic field was removed, which indicated the orientational ordering of NPLs. We used a system of three pairs of coils to compensate the Earth magnetic field to values below around 1 μT. Second, a small magnetic probing field was used to change the direction of average orientation of NPLs as shown in Fig. S3, which means that the NPLs were also magnetically ordered, i.e., the sample exhibited magnetization. Third, in the absence of a magnetic field, the sample formed a polydomain structure with clearly visible domain walls (similar to Scheme 1). The structure, where magnetization in different domains points in different directions, minimizes the magnetic stray field and indicates that the magnetization is not externally induced, but inherent and spontaneous, i.e., such a sample is ferromagnetic.

3. Results and discussion

3.1. Surface functionalization of magnetic NPLs

Two types of the core BSHF NPLs, i.e., BSHF-a and BSHF-b, were synthesized. They were of typical platelike shape with diameters between 10 and 150 nm, a mean diameter of around 50 nm, and thicknesses of around 3–5 nm (Fig. S1). Their structure corresponded to that of the barium hexaferrite. The constituent elements were confirmed with energy dispersive X-ray spectroscopy (EDXS; as an example, see Fig. S2). Both NPLs show a typical magnetic hysteresis at room temperature with coercivities of 77 kA/m (BSHF-a) and 94 kA/m BSHF-b,

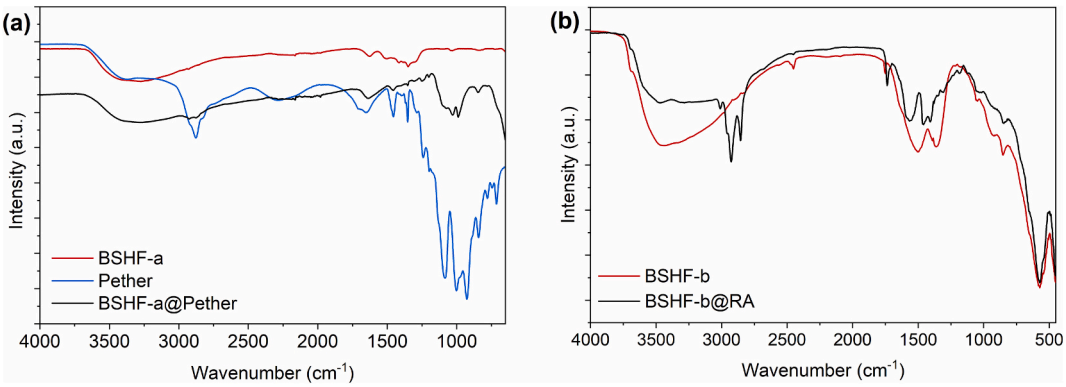

Fig. 1. FTIR spectra of the core and functionalized BSHF NPLs with: (a) Pether and (b) RA.

and saturation magnetization of 35 Am^2/kg (BSHF-a) and 33 Am^2/kg (BSHF-b). The measured saturation magnetization is roughly 10 % lower than the actual saturation magnetization (39 Am^2/kg and 37 Am^2/kg for BHSF-a and BSHF-b, respectively) due to the nonmagnetic adsorbents such as water, carbonates, and in the BSHF-a NPLs, also nitrates (see Figs. 1 and 4).

The adsorption of Pether onto the BSHF-a NPLs was inferred from their superior colloidal stability in water when compared to the original aqueous suspension of the core NPLs. While some sedimentation was observed when concentrating the aqueous suspension of the core NPLs above ~20 mg/ml this was not so for the NPLs functionalized with Pether. In addition, phosphorus from the ligand was detected together with other constituent elements by EDXS (Fig. S2). The presence of Pether in the functionalized NPLs was also indicated from the ATR-FTIR spectrum (Fig. 1a). The spectrum of the core BSHF-a NPLs contains a wide band at ~3500–3000 cm^{-1} that can be associated with adsorbed water [29,30], the lower intensity bands at around 1630 and 1520 cm^{-1} correspond to the adsorbed CO_2 and the bands at around 1350–1400 cm^{-1} to N—O from HNO_3 [31,32]. The phosphonic group bands, P═O, P–O–H and P—C are in the range of 1085–712 cm^{-1} [33–35] and are observed in the spectrum of the pure ligand and of the BSHF-a@Pether NPLs. These bands overlap with the C—O stretching band of the ether groups at ~1100 cm^{-1}.

Similar to the above, the adsorption of RA on the BSHF-b NPLs was inferred from the colloidal stability of the functionalized NPLs in the low-polar solvents. Namely, the core BSHF-b NPLs have a hydrophilic surface and agglomerate in low-polar solvents. Another evidence of the RA in the functionalized NPLs was obtained from the DRIFT spectrum (Fig. 1b). The bands in the spectrum of core BSHF-b NPLs can be associated with Fe—O at ~580 and below 450 cm^{-1} [36], the bands at ~1500 and ~ 1360 cm^{-1} to the adsorbed carbonate [37] and the wide band at ~3500–3000 cm^{-1} can be associated with adsorbed water [29,30]. The broad band at ~3500–3000 cm^{-1} is less intense in the functionalized BSHF-b NPLs, suggesting that water molecules were exchanged by RA and the band can be attributed to C—H of the fatty acid [34]. The bands at ~2920 and ~ 2840 cm^{-1} correspond to stretching of the aliphatic chain (C—H and CH_2) and the bands at ~1740–1410 cm^{-1} correspond to C═O, in particular to the carboxyl group (C═O, COO^- and $–CH_2CO–$) [34,38].

3.2. Ferromagnetic FFs

An aqueous ferromagnetic FF from the BSHF-a@Pether NPLs was prepared by concentrating the initial FF (<5 mg/ml) obtained immediately after the surface functionalization of the core NPLs (see Materials and methods). The ferromagnetic FFs in low-polar solvents were obtained by dispersing the RA-functionalized NPLs in a low volume of the solvent. A minor fraction of the NPLs sedimented in a few days and were separated from the supernatant. The final concentration of the BSHF-b@RA NPLs in the supernatant was 83 mg/ml (~1.6 vol%) in DCM and 88 mg/ml (~1.7 vol%) in 1-hexanol. The DCM FF was ferromagnetic as-prepared, while the 1-hexanol and the aqueous suspensions were additionally concentrated by a magnet in a glass capillary used for the polarized optical microscope (POM) observations. Under POM, all the samples appeared bright under crossed polarisers and exhibited homogeneous texture with visible fluctuations, indicating their fluidic nature. All samples exhibited magneto-optic response and could be ordered into a single domain sample with homogeneous texture via magnetic fields in the order of 10 mT. For all three systems, we were able to observe distinct magnetic domains with clearly visible domain walls at a zero external magnetic field (Fig. 2). This indicates that the NPLs are ordered locally into a ferromagnetic nematic FF.

3.2.1. Mechanism of the colloidal stability in aqueous ferromagnetic FFs

The magnetic nanoparticles with very low or no remanent magnetization (superparamagnetic nanoparticles) are colloidally stabilized in

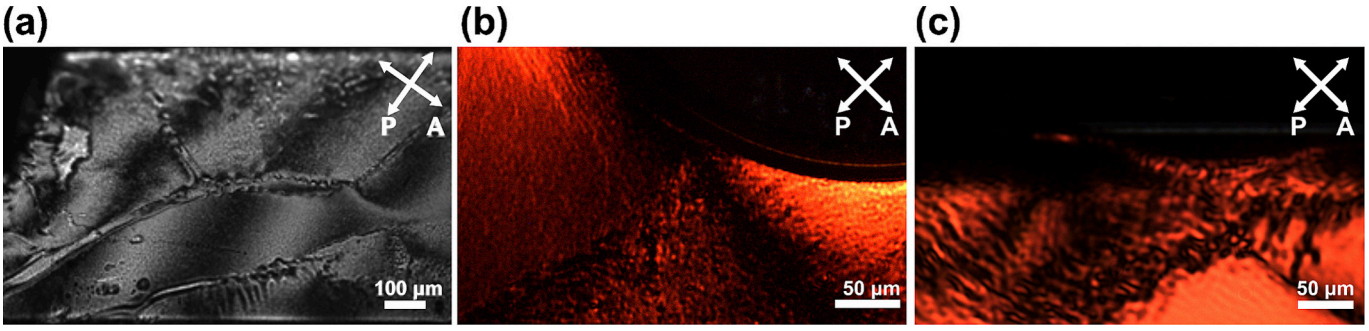

Fig. 2. POM images taken at a zero magnetic field of the ferromagnetic FF in: (a) water and (b) DCM, and (c) 1-hexanol. For clarity, the brightness and contrast of (b) photograph are here increased; the original photograph is shown in Fig. S3.

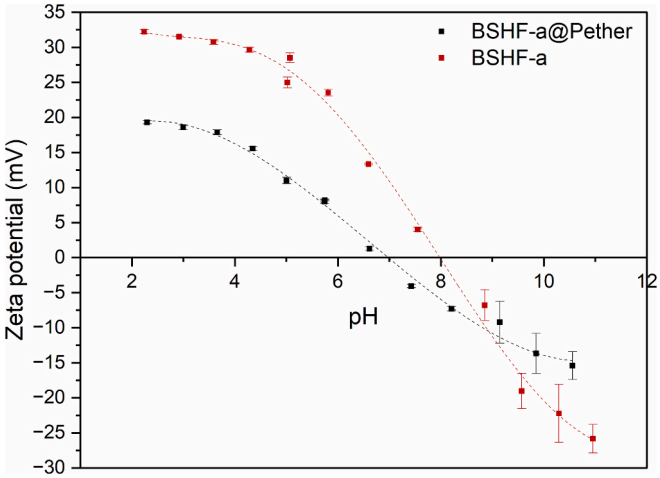

Fig. 3. Zeta-potential behaviour vs pH of the BSHF-a and BSHF-a@Pether aqueous FF.

various liquids, similarly to nonmagnetic particles [39]. Van der Waals forces are the only attractive colloidal forces responsible for their agglomeration. The latter can be prevented with electrostatic, steric, or electrosteric repulsive forces by optimizing the surface chemistry of the nanoparticles. However, the main attractive interaction between the permanently magnetic BSHF NPLs is a magnetic dipolar attraction [12], which is of a longer range than the van der Waals forces. Therefore, repulsive forces of a sufficiently long range are needed for stabilizing the BSHF NPLs.

The electrostatic interaction between the NPLs in the studied aqueous system was inferred from the electrokinetic measurements. The point of zero charge (PZC) of the core BSHF-a NPLs at $pH_{PZC} \sim 8$ falls between the one for the goethite (α-FeO(OH)) [40,41] and hematite (α-Fe_2O_3) [42,43], implying that the surface sites were not fully hydroxylated [44]. The dilution of the surface hydroxyl sites of the BSHF-a NPLs after the functionalization with Pether molecules resulted in lower absolute values of the zeta potential in the whole measured pH range (Fig. 3). Moreover, the PZC of the BSHF-a@Pether decreased to $pH_{PZC} \sim 7$, i.e., similar to hematite, which is consistent with the lower surface density of hydroxyl sites. A similar decrease in the pH_{ZPC} was previously associated with the coordination of the surface metal ions with catechols [45,46].

The mass fraction of the ligand in BSHF-a@Pether NPLs from the as-obtained aqueous FF was 12.5 % and was determined from the TGA mass loss associated with the organic fragments detected using MS, such as *m/z* 15 of CH_3^+, m/z 44 of CO_2, m/z 31 of OCH_3^+, and m/z 45 of $CH_2OCH_3^+$ (Fig. 4a). This 12.5 wt% correlates roughly with a surface density of 3 molecules/nm^2, which is, theoretically, the maximum possible surface density of phosphonic groups on the BSHF NPLs [47]. This means that approximately one-third (i.e., 3/10) of the surface Fe (III) ions [48] are coordinated with Pether via its phosphonic group. This represents a significant change in the surface site occupancy considering the core BSHF-a NPLs and explains the significant change in the zeta-potential behaviour of the NPLs after their functionalization (Fig. 3).

Regardless of the exact surface chemistry of the BSHF-a@Pether NPLs, their stability in water cannot be attributed solely to the electrostatic repulsion as in the case of the first ferromagnetic ferrofluids in 1-butanol (Table 1). Namely, the core BSHF-a NPLs with a higher absolute zeta potential started to sediment in water at concentrations above 20 mg/ml. Therefore, an additional repulsive interaction to the electrostatic repulsion, in particular, a combined hydration of the Pether surface ligands and steric repulsion, must have enabled aqueous ferromagnetic FFs. Ethers and polyethers are well hydrated by water molecules [22], which can enhance the steric repulsion. For a well-hydrated dense assembly of Pether molecules, the total repulsive interaction is sufficient to enable the nematic ordering of the NPLs and the ferromagnetic coupling while, at the same time, preventing their irreversible agglomeration (Scheme 2a). While the NPLs are only weakly (i.e., reversibly) flocculated in the nematic phase, they would irreversibly

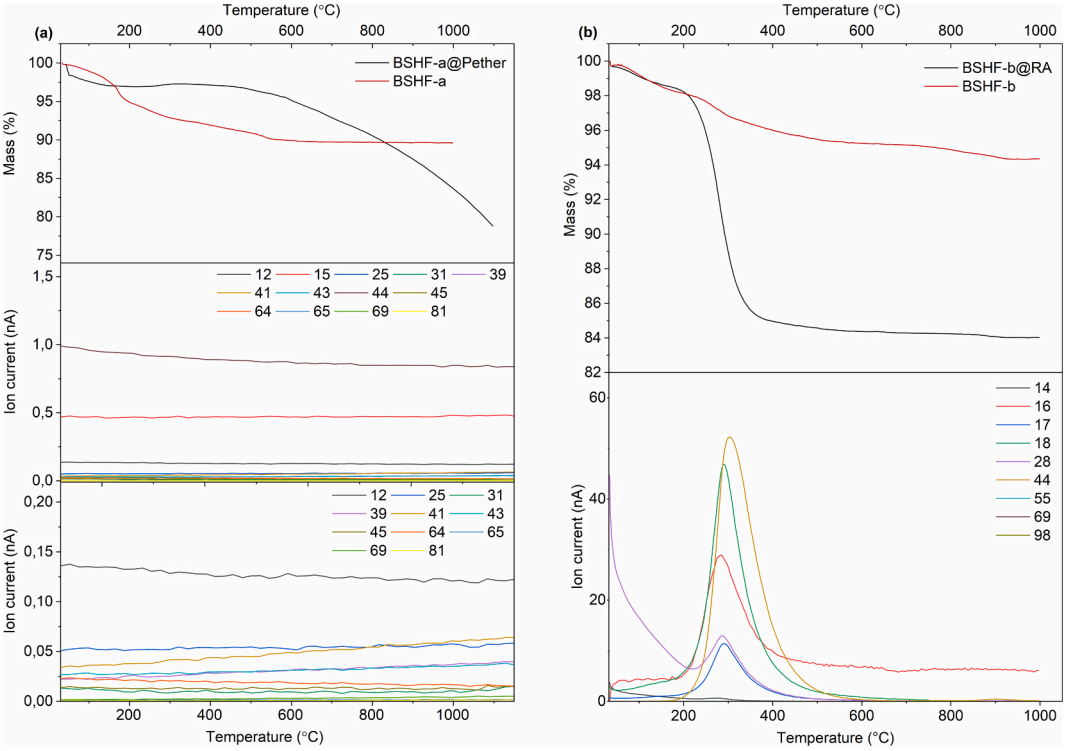

Fig. 4. TGA curves (top) of the core and functionalized NPLs with corresponding MS spectra (centre and bottom) of the functionalized NPLs: (a) BSHF-a@Pether and (b) BSHF-b@RA. The legend in MS spectra depicts the *m/z* values. The MS spectrum in panel (a) was zoomed (bottom) for the m/z with low intensities (centre).

Table 1
List of the ferromagnetic ferrofluids composed of BHF NPLs in isotropic solvents, with the stabilization mechanism, and origin of ferromagnetic (FM) order.

Medium	Stabilization mechanism	Origin of the FM order	References
1-butanol	Electrostatic repulsion by the surface DBSa double layer	Equilibrated magnetic dipolar interaction with the electrostatic repulsion	[4,13]
Water	Combined electrostatic and hydration repulsion of Pether at the NPLs	Equilibrated magnetic dipolar interaction with the electrostatic and hydration repulsion	This work
DCM	Combined steric and solvation repulsion	Equilibrated magnetic dipolar interaction with the steric and solvation repulsion	This work
1-hexanol	Combined steric and solvation repulsion	Equilibrated magnetic dipolar interaction with the steric and solvation repulsion	This work

agglomerate in the absence of a sufficient repulsive interaction. In the latter case, the dominating magnetic dipolar attraction induces the formation of robust columnar agglomerates.

3.2.2. *Mechanism of the colloidal stability in low-polar ferromagnetic FFs*

As expected, negligible zeta potential and conductivity were measured in low-polar FFs with BSHF-b@RA. Their colloidal stability was assessed visually and by dynamic light scattering (DLS) measurements. Both FFs were dark (due to the high concentration of NPLs) and shiny (Fig. S4), indicating the dispersed NPLs with flat surfaces. A solvodynamic size distribution of the NPLs@RA in both solvents does not exceed the equivalent diameter range determined from the TEM images (Fig. 5), which would indicate the presence of aggregates. Somewhat lower solvodynamic size can be attributed to the fact that the DLS method does not distinguish between the thickness (~3–5 nm) and the diameter of the NPLs. Nevertheless, it is inferred from the equivalent diameter distribution that the DCM ferrofluid contains larger NPLs than the 1-hexanol. Moreover, the equivalent diameter distribution of the BSHF-b@RA NPLs in DCM is similar to that of the as-synthesized core BSHF-b NPLs (Fig. S1d), while the fraction of the widest NPLs (>80 nm) is not present in the 1-hexanol FF. The NPL's magnetic moment and, with it, the magnetic dipolar interaction both increase with the NPL's volume. This explains why, despite the similar NPL concentration (~1.7 vol%) in both solvents, the magnetic domains were observable already in the as-prepared DCM FF, while the 1-hexanol FF had to be additionally concentrated in the capillary before the POM observation. Namely, the larger NPLs possess larger magnetic moments, and the ferromagnetic interaction between them is stronger (at a longer distance) than between the smaller NPLs [13].

The mass fraction of RA in the BSHF-b@RA NPLs was determined directly from the mass loss at 150–400 °C with TGA since RA decomposes completely up to 400 °C (Fig. 4b). The decomposition of RA was correlated with the m/z = 43 ($C_3H_7^+$), 55 ($C_4H_7^+$ or $C_3H_3O^+$), 69 ($C_5H_9^+$), 82 ($C_5H_6O^+$), 97 ($C_6H_9O^+$), 98 ($C_6H_{10}O^+$) fragments in the MS spectrum. The mass fraction of RA was similar in both nonpolar ferromagnetic FFs, i.e., 13.68 wt% in DCM and 16.09 wt% in 1-hexanol. The determined mass fraction of RA accounts for the total RA from the FFs, i.e., the adsorbed and dissolved molecules. The equilibrium between the adsorbed and dissolved RA is the key to the colloidal stability of these dispersions.

Due to negligible electrostatic interaction in low-polar solvents, the observed excellent colloidal stability of the BSHF-b@RA was not expected. In all known FFs of the permanently magnetic BSHF NPLs, including the first ferromagnetic FF [4,13], the sufficiently long-range electrostatic interaction between the charged surfaces of the NPLs stabilized the system [17,18,47]. The steric repulsion by the RA molecules alone has a relatively short range (i.e., ~2 nm for a monolayer) in comparison to the range of the magnetic dipolar interaction (>10 nm [12]). Therefore, we assume that in the low-polar systems, the steric repulsion must have been magnified by a solvation interaction (Table 1), preventing the irreversible agglomeration of the NPLs (Scheme 2b).

To assess the effect of a solvent, we examined some other low-polar solvents. According to Gyerygek [25], larger concentrations of NPLs were expected in less polar solvents than DCM ($\varepsilon = 8.93$). Indeed, FFs of ultra-high concentrations of the BSHF-b@RA NPLs (~220 mg/ml ~ 4 vol%) were obtained in chloroform ($\varepsilon = 4.81$); however, under POM no clear formation of magnetic domains was observed, hence we were unable to confirm the ferromagnetic ordering in the chloroform dispersion. The absence of FM phase could stem from partial agglomeration of the NPLs (ε of chloroform is lower than that of DCM or 1-hexanol) or from gelation of the dispersion. We are currently investigating this system in detail to elucidate these results. While the construction of a complete phase diagram and examination of the dispersion across a broad concentration range might reveal domain formation, such an investigation lies outside the scope of the present work. In the solvents of even lower polarity than that of chloroform, such as hexylamine (ε =

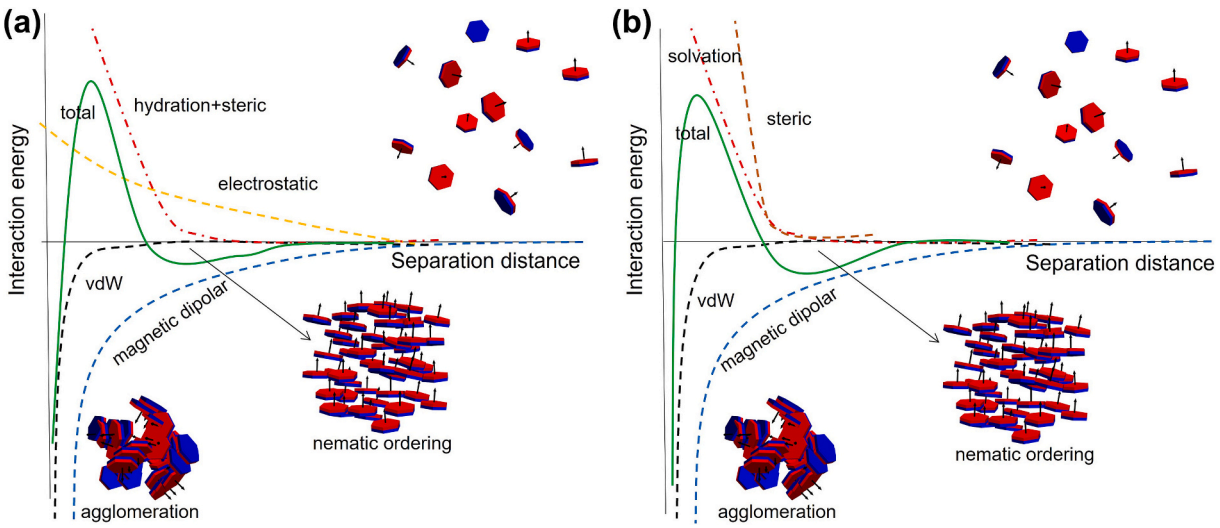

Scheme 2. Schematics of the colloidal stabilization of ferromagnetic FFs: (a) aqueous from the BSHF-a@Pether and (b) nonpolar from the BSHFb@RA. The NPLs are weakly (i.e., reversibly) flocculated, i.e., nematic phase, in the secondary minimum that does not exceed the thermal energy (< kT), whereas the repulsive interaction prevents NPLs from irreversible agglomeration in the primary minimum (> > kT).

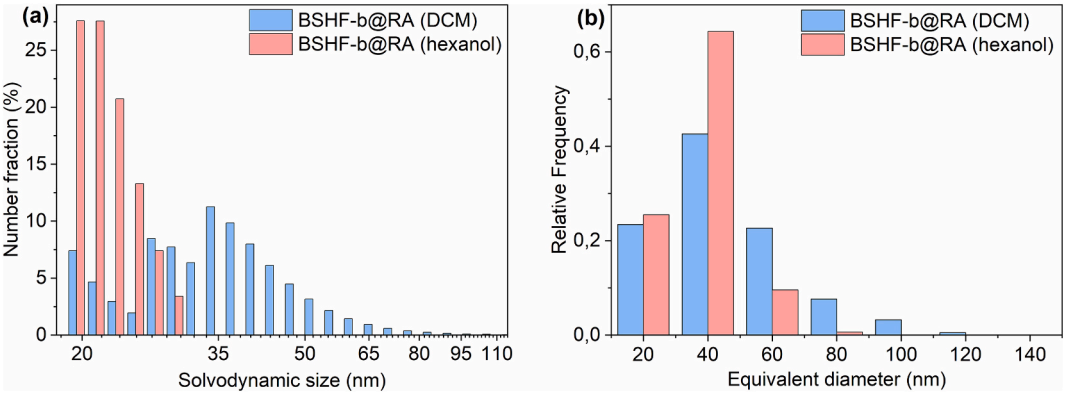

Fig. 5. Size distribution of the NPLs from the suspensions in low-polar solvents: (a) solvodynamic size determined with DLS and (b) equivalent diameter determined from the TEM images.

4.08) or toluene (ε = 2.38), the BSHF@RA NPLs were stable only at significantly lower concentrations (5 mg/ml ~0.1 vol% in hexylamine and 30 mg/ml ~0.6 vol% in toluene). Our results show that DCM with a dielectric constant of 8.93 is the best solvent (among the studied) for preparing ferromagnetic FFs, while 1-hexanol (ε = 13.30) is the most polar solvent enabling the formation of the ferromagnetic nematic phase from the BSHF@RA NPLs.

4. Conclusion

We developed two new ferromagnetic ferrofluid (FF) systems, one in water and the other in low-polar solvents. In addition to the first ferromagnetic FF in 1-butanol [4], these are the only known room-temperature ferromagnetic liquids in isotropic solvents (Table 1). All these systems contain permanently magnetic nanoplatelets (NPLs) based on barium hexaferrite. At a sufficiently high concentration, the NPLs order locally into a ferromagnetic nematic phase in which magnetic domains evolve in the absence of an applied magnetic field. In the aqueous ferromagnetic FF, the NPLs are functionalized with a phosphonic polyether. In the so-functionalized NPLs, the long-range magnetic dipolar attraction is equilibrated by combined repulsive electrostatic, steric, and hydration interactions. The low-polar ferromagnetic FFs are composed of the NPLs functionalized with ricinoleic acid in dichloromethane or 1-hexanol. Their colloidal stability comes from a sufficient steric repulsion induced through a solvation interaction of the surface ricinoleic-acid molecules with the solvent. This study broadens the conceptual and practical framework for designing ferromagnetic ferrofluids and opens new possibilities for their application in microscale magnetic actuation such as [15,16]. The newly designed suspensions broaden this applicability to microfluidic environments where compatibility with either aqueous or hydrophobic phases is required.

CRediT authorship contribution statement

Jošt Tručl: Writing – review & editing, Writing – original draft, Methodology, Formal analysis. **Patricija Hribar Boštjančič:** Writing – review & editing, Methodology, Formal analysis. **Žiga Gregorin:** Writing – review & editing, Formal analysis. **Peter Medle Rupnik:** Writing – review & editing, Formal analysis. **Alenka Mertelj:** Writing – review & editing, Supervision, Conceptualization. **Darja Lisjak:** Writing – review & editing, Writing – original draft, Supervision, Formal analysis, Conceptualization.

Funding

The study was partly funded by Slovenian Research and Innovation Agency research core funding P2–0089 and P1–0192, and the research

project PR-12851. The study was also partly funded from the MAGNELIQ project. The project has received funding from the European Union's Horizon 2020 research and innovation under grant agreement No 899285.

Declaration of competing interest

The authors declare that they have no known competing financial interests or personal relationships that could have appeared to influence the work reported in this paper.

Acknowledgments

Authors acknowledge the financial support from the Slovenian Research and Innovation Agency through the research core funding P2-0089 and P1-0192, and the research project PR-12851. The study was partly funded from the MAGNELIQ project. The project has received funding from the European Union's Horizon 2020 research and innovation under grant agreement No 899285. The results reflect only the authors' view and the Commission is not responsible for any use that may be made of the information it contains.

We also acknowledge access to TEM (Jeol 2100) and VSM at CENN Nanocenter.

Additionally, we thank Marjeta Maček Kržmanc for the thermogravimetric analysis and Slavko Kralj for the critical review of the manuscript.

Appendix A. Supplementary data

Supplementary data to this article can be found online at https://doi.org/10.1016/j.jcis.2025.138806.

Data availability

Data is available at https://doi.org/10.5281/zenodo.15654897

References

[1] D.N. Paulson, J.C. Wheatley, Evidence for electronic ferromagnetism in superfluid 3He-A, Phys. Rev. Lett. 40 (1978) 557–561, https://doi.org/10.1103/PhysRevLett.40.557.

[2] T. Albrecht, C. Bührer, M. Fähnle, K. Maier, D. Platzek, J. Reske, First observation of ferromagnetism and ferromagnetic domains in a liquid metal, Appl. Phys. A 65 (1997) 215–220, https://doi.org/10.1007/s003390050569.

[3] A. Mertelj, D. Lisjak, M. Drofenik, M. Čopič, Ferromagnetism in suspensions of magnetic platelets in liquid crystal, Nature 504 (2013) 237–241, https://doi.org/10.1038/nature12863.

[4] M. Shuai, A. Klittnick, Y. Shen, G.P. Smith, M.R. Tuchband, C. Zhu, R.G. Petschek, A. Mertelj, D. Lisjak, M. Čopič, J.E. Maclennan, M.A. Glaser, N.A. Clark, Spontaneous liquid crystal and ferromagnetic ordering of colloidal magnetic nanoplates, Nat. Commun. 7 (2016), https://doi.org/10.1038/ncomms10394.

[5] F. Brochard, P.G. de Gennes, Theory of magnetic suspensions in liquid crystals, J. Phys. 31 (1970) 691–708, https://doi.org/10.1051/JPHYS:01970003107069100.

[6] S.H. Chen, N.M. Amer, Observation of macroscopic collective behavior and new texture in magnetically doped liquid crystals, Phys. Rev. Lett. 51 (1983) 2298, https://doi.org/10.1103/PhysRevLett.51.2298.

[7] P. Kopčanský, N. Tomašovičová, M. Koneracká, V. Závišová, M. Timko, A. Džarová, A. Šprincová, N. Iber, K. Fodor-Csorba, T. Tóth-Katona, A. Vajda, J. Jadzyn, Structural changes in the 6CHBT liquid crystal doped with spherical, rodlike, and chainlike magnetic particles, Phys. Rev. E Stat. Nonlinear Soft Matter Phys. 78 (2008) 011702, https://doi.org/10.1103/PHYSREVE.78.011702/FIGURES/10/MEDIUM.

[8] N. Podoliak, O. Buchnev, D.V. Bavykin, A.N. Kulak, M. Kaczmarek, T.J. Sluckin, Magnetite nanorod thermotropic liquid crystal colloids: synthesis, optics and theory, J. Colloid Interface Sci. 386 (2012) 158–166, https://doi.org/10.1016/j.jcis.2012.07.082.

[9] D. Lisjak, A. Mertelj, Anisotropic magnetic nanoparticles: a review of their properties, syntheses and potential applications, Prog. Mater. Sci. 95 (2018) 286–328, https://doi.org/10.1016/J.PMATSCI.2018.03.003.

[10] H. Nádasi, P. Medle Rupnik, M. Küster, A. Jarosik, R. Tuffin, M. Bremer, M. Klasen-Memmer, D. Lisjak, N. Sebastián, A. Mertelj, F. Ludwig, A. Eremin, Room-Temperature Multiferroic Liquids: Ferroelectric and Ferromagnetic Order in a Hybrid Nanoparticle–Liquid Crystal System, Adv. Mater. (2025) e08406, https://doi.org/10.1002/ADMA.202508406;SUBPAGE:STRING:FULL.

[11] Ž. Gregorin, N. Sebastián, N. Osterman, P. Hribar Boštjančič, D. Lisjak, A. Mertelj, Dynamics of domain formation in a ferromagnetic fluid, J. Mol. Liq. 366 (2022) 120308, https://doi.org/10.1016/j.molliq.2022.120308.

[12] P. Hribar Boštjančič, M. Tomšič, A. Jamnik, D. Lisjak, A. Mertelj, Electrostatic interactions between barium Hexaferrite Nanoplatelets in alcohol suspensions, J. Phys. Chem. C 123 (2019) 23272–23279, https://doi.org/10.1021/acs.jpcc.9b07455.

[13] P. Hribar Boštjančič, Ž. Gregorin, N. Sebastián, N. Osterman, D. Lisjak, A. Mertelj, Isotropic to nematic transition in alcohol ferrofluids of barium hexaferrite nanoplatelets, J. Mol. Liq. 348 (2022) 118038, https://doi.org/10.1016/j.molliq.2021.118038.

[14] M. Vilfan, B. Lampret, Ž. Gregorin, L. Cmok, A. Vilfan, J. Klepp, J. Kohlbrecher, P. Hribar Boštjančič, D. Lisjak, A. Mertelj, Spontaneous chiral symmetry breaking and lane formation in ferromagnetic Ferrofluids, Small 19 (2023) 2304387, https://doi.org/10.1002/smll.202304387.

[15] X. Liu, N. Kent, A. Ceballos, R. Streubel, Y. Jiang, Y. Chai, P.Y. Kim, J. Forth, F. Hellman, S. Shi, D. Wang, B.A. Helms, P.D. Ashby, P. Fischer, T.P. Russell, Reconfigurable ferromagnetic liquid droplets, Science 365 (2019) (1979) 264–267, https://doi.org/10.1126/science.aaw8719.

[16] L. Mao, H. Koser, Towards ferrofluidics for μ-TAS and lab on-a-chip applications, Nanotechnology 17 (2006) S34, https://doi.org/10.1088/0957-4484/17/4/007.

[17] S. Ovtar, D. Lisjak, M. Drofenik, Barium hexaferrite suspensions for electrophoretic deposition, J. Colloid Interface Sci. 337 (2009) 456–463, https://doi.org/10.1016/j.jcis.2009.05.041.

[18] T. Goršak, D. Makovec, U. Javornik, B. Belec, S. Kralj, D. Lisjak, A functionalization strategy for the dispersion of permanently magnetic barium-hexaferrite nanoplatelets in complex biological media, Colloids Surf. A Physicochem. Eng. Asp. 573 (2019) 119–127, https://doi.org/10.1016/j.colsurfa.2019.04.051.

[19] C. Queffélec, M. Petit, P. Janvier, D.A. Knight, B. Bujoli, Surface modification using Phosphonic acids and esters, Chem. Rev. 112 (2012) 3777–3807, https://doi.org/10.1021/cr2004212.

[20] G. Guerrero, J.G. Alauzun, M. Granier, D. Laurencin, P.H. Mutin, Phosphonate coupling molecules for the control of surface/interface properties and the synthesis of nanomaterials, Dalton Trans. 42 (2013) 12569–12585, https://doi.org/10.1039/C3DT51193F.

[21] S. Pawsey, M. McCormick, S. De Paul, R. Graf, Y.S. Lee, L. Reven, H.W. Spiess, 1H fast MAS NMR studies of hydrogen-bonding interactions in self-assembled monolayers, J. Am. Chem. Soc. 125 (2003) 4174–4184, https://doi.org/10.1021/ja029008u.

[22] B. Ensing, A. Tiwari, M. Tros, J. Hunger, S.R. Domingos, C. Pérez, G. Smits, M. Bonn, D. Bonn, S. Woutersen, On the origin of the extremely different solubilities of polyethers in water, Nat. Commun. 10 (2019) 2893, https://doi.org/10.1038/s41467-019-10783-z.

[23] H. Dietrich, S. Scheiner, L. Portilla, D. Zahn, M. Halik, Improving the performance of organic thin-film transistors by ion doping of ethylene-glycol-based self-assembled monolayer hybrid dielectrics, Adv. Mater. 27 (2015) 8023–8027, https://doi.org/10.1002/adma.201503911.

[24] D. Lisjak, M. Drofenik, Chemical substitution—an alternative strategy for controlling the particle size of barium ferrite, Cryst. Growth Des. 12 (2012) 5174–5179, https://doi.org/10.1021/cg301227r.

[25] S. Gyergyek, D. Makovec, M. Drofenik, Colloidal stability of oleic- and ricinoleic-acid-coated magnetic nanoparticles in organic solvents, J. Colloid Interface Sci. 354 (2011) 498–505, https://doi.org/10.1016/j.jcis.2010.11.043.

[26] K. Williamson, K.T. Møller, A.M. D'Angelo, T.D. Humphries, M. Paskevicius, C. E. Buckley, Thermochemical energy storage in barium carbonate enhanced by iron (iii) oxide, Phys. Chem. Chem. Phys. 25 (2023) 7268–7277, https://doi.org/10.1039/D2CP05745J.

[27] D. Lisjak, P. Hribar Boštjančič, A. Mertelj, A. Mavrič, M. Valant, J. Kovač, H. Hudelja, A. Kocjan, D. Makovec, Formation of Fe(III)-phosphonate coatings on barium Hexaferrite Nanoplatelets for porous Nanomagnets, ACS, Omega 5 (2020) 14086–14095, https://doi.org/10.1021/acsomega.0c01597.

[28] P.C. Hiemenz, R. Rajagopalan, Principles of Colloid and Surface Chemistry, 3rd ed., Marcel Dekker, New York, 1997.

[29] C.S. Pauly, A.-C. Genix, J.G. Alauzun, M. Sztucki, J. Oberdisse, P. Hubert Mutin, Surface modification of alumina-coated silica nanoparticles in aqueous sols with phosphonic acids and impact on nanoparticle interactions, Phys. Chem. Chem. Phys. 17 (2015) 19173–19182, https://doi.org/10.1039/C5CP01925G.

[30] R.M.P. Colodrero, G.K. Angeli, M. Bazaga-Garcia, P. Olivera-Pastor, D. Villemin, E. R. Losilla, E.Q. Martos, G.B. Hix, M.A.G. Aranda, K.D. Demadis, A. Cabeza, Structural variability in multifunctional metal Xylenediaminetetraphosphonate hybrids, Inorg. Chem. 52 (2013) 8770–8783, https://doi.org/10.1021/ic400951s.

[31] I.E. Wachs, Infrared spectroscopy of supported metal oxide catalysts, Colloids Surf. A Physicochem. Eng. Asp. 105 (1995) 143–149, https://doi.org/10.1016/0927-7757(95)03325-5.

[32] K.I. Hadjiivanov, Identification of neutral and charged N x O y surface species by IR spectroscopy, Catal. Rev. 42 (2000) 71–144, https://doi.org/10.1081/CR-100100260.

[33] Y. Lalatonne, C. Paris, J.M. Serfaty, P. Weinmann, M. Lecouvey, L. Motte, Bis-phosphonates–ultra small superparamagnetic iron oxide nanoparticles: a platform towards diagnosis and therapy, Chem. Commun. (2008) 2553–2555, https://doi.org/10.1039/B801911H.

[34] G. Socrates, Infrared and Raman Characteristic Group Frequencies: Tables and Charts, John Wiley & Sons Ltd, Chichester, 1994.

[35] T.J. Daou, S. Begin-Colin, J.M. Grenèche, F. Thomas, A. Derory, P. Bernhardt, P. Legaré, G. Pourroy, Phosphate adsorption properties of magnetite-based nanoparticles, Chem. Mater. 19 (2007) 4494–4505, https://doi.org/10.1021/cm071046v.
[36] K.K. Bamzai, G. Kour, B. Kaur, M. Arora, R.P. Pant, Infrared spectroscopic and electron paramagnetic resonance studies on Dy substituted magnesium ferrite, J. Magn. Magn. Mater. 345 (2013) 255–260, https://doi.org/10.1016/j.jmmm.2013.07.002.
[37] H. Wijnja, C.P. Schulthess, ATR–FTIR and DRIFT spectroscopy of carbonate species at the aged γ-Al2O3/water interface, Spectrochim. Acta A Mol. Biomol. Spectrosc. 55 (1999) 861–872, https://doi.org/10.1016/S1386-1425(98)00236-4.
[38] E. Andresen, C. Würth, C. Prinz, M. Michaelis, U. Resch-Genger, Time-resolved luminescence spectroscopy for monitoring the stability and dissolution behaviour of upconverting nanocrystals with different surface coatings, Nanoscale 12 (2020) 12589–12601, https://doi.org/10.1039/D0NR02931A.
[39] J. Israelachvili, Intermolecular and Surface Forces, 3rd edition, 2011.
[40] F. Gaboriaud, J.-J. Ehrhardt, Effects of different crystal faces on the surface charge of colloidal goethite (α-FeOOH) particles: an experimental and modeling study, Geochim. Cosmochim. Acta 67 (2003) 967–983, https://doi.org/10.1016/S0016-7037(02)00988-2.
[41] A.J.A. Aquino, D. Tunega, G. Haberhauer, M.H. Gerzabek, H. Lischka, Acid–base properties of a goethite surface model: a theoretical view, Geochim. Cosmochim. Acta 72 (2008) 3587–3602, https://doi.org/10.1016/j.gca.2008.04.037.
[42] R.C. Plaza, J.L. Arias, M. Espín, M.L. Jiménez, A.V. Delgado, Aging effects in the Electrokinetics of colloidal Iron oxides, J. Colloid Interface Sci. 245 (2002) 86–90, https://doi.org/10.1006/jcis.2001.7964.
[43] L. Čerović, G. Lefèvre, A. Jaubertie, M. Fédoroff, S. Milonjić, Deposition of hematite particles on polypropylene walls in dynamic conditions, J. Colloid Interface Sci. 330 (2009) 284–291, https://doi.org/10.1016/j.jcis.2008.10.079.
[44] M. Poberžnik, G. Herrero-Saboya, D. Makovec, D. Lisjak, L. Martin-Samos, Surface phase diagrams of pristine and hydroxylated barium hexaferrite surfaces from first-principles atomistic thermodynamics, Appl. Surf. Sci. 637 (2023) 157890, https://doi.org/10.1016/j.apsusc.2023.157890.
[45] S. Čampelj, M. Pobrežnik, T. Landovsky, J. Kovač, L. Martin-Samos, V. Hamplova, D. Lisjak, The influence of Catechols on the magnetization of Iron oxide nanoparticles, Nanomaterials 13 (2023), https://doi.org/10.3390/nano13121822.
[46] R. Rodríguez, M.A. Blesa, A.E. Regazzoni, Surface complexation at the TiO2 (anatase)/aqueous solution Interface: chemisorption of catechol, J. Colloid Interface Sci. 177 (1996) 122–131, https://doi.org/10.1006/jcis.1996.0012.
[47] A. Tufani, N. Popov, J. Kovač, S. Čampelj, A. Mavrič, T. Landovský, M. Cigl, P. Vaňkátová, M. Loula, V. Novotná, M. Poberžnik, G. Herrero-Saboya, L. Martin-Samos, A. Mertelj, D. Lisjak, Nonconductive ferrofluids from permanently magnetic nanoplatelets hybridized with polar phosphonic ligands, Dalton Trans. 54 (2025) 7906–7922, https://doi.org/10.1039/D5DT00281H.
[48] D. Makovec, M. Komelj, G. Dražić, B. Belec, T. Goršak, S. Gyergyek, D. Lisjak, Incorporation of Sc into the structure of barium-hexaferrite nanoplatelets and its extraordinary finite-size effect on the magnetic properties, Acta Mater. 172 (2019) 84–91, https://doi.org/10.1016/j.actamat.2019.04.050.